Available online at www.sciencedirect.com
SCIENCE DIRECT®
Journal of Solid State Chemistry 177 (2004) 4508–4515
JOURNAL OF SOLID STATE CHEMISTRY
www.elsevier.com/locate/jssc

Synthesis and characterization of sodium titanates $Na_2Ti_3O_7$ and $Na_2Ti_6O_{13}$

A-L. Sauvet, S. Baliteau, C. Lopez*, P. Fabry

Laboratoire d'Electrochimie et de Physico-Chimie des Matériaux et des Interfaces, UMR 5631 CNRS-INPG-UJF, ENSEEG, 1130 rue de la Piscine, BP 75, 38402 Saint Martin d'Hères, France

Received 30 July 2004; received in revised form 9 September 2004; accepted 10 September 2004
Available online 11 November 2004

Abstract

$Na_2Ti_3O_7$ and $Na_2Ti_6O_{13}$ were synthesized by sol–gel method in order to obtain pure phases. Different heat-treatments were applied on powders and pellets of these materials. The effects were studied by XRD, dilatometry, TGA-DTA, SEM and electrochemical impedance spectroscopy. Pure $Na_2Ti_3O_7$ was obtained at 973 K. Sintering at 1373 K caused a partial decomposition into $Na_2Ti_6O_{13}$. The $Na_2Ti_3O_7$ powder sintered at 1273 K showed polygonal microstructure. $Na_2Ti_3O_7$ pellets sintered at 1323 K for 10 h exhibited large structures. This latter microstructure decreased the electrical conductivity of $Na_2Ti_3O_7$. Pure $Na_2Ti_6O_{13}$ was obtained at 873 K. Sintering at 1073 K caused a partial decomposition into TiO_2 (rutile). $Na_2Ti_6O_{13}$ pellets sintered at 1323 K for 10 h exhibited common shrinkage behavior. This shrinkage process increased the electrical conductivity of this material. The presence of TiO_2 resulted in a oxygen partial pressure dependence of the electrical conductivity.

Keywords: Sodium titanates; Structural characterization; EIS; Conductivity

1. Introduction

Alkali and alkaline earth titanates are used in several applications [1] and they were proposed as materials for oxygen electrodes in potentiometric sensors for CO_2 and O_2 [2–5].

The alkali-metal titanates $A_2Ti_nO_{2n+1}$ ($n=3$ or 8, and A = Na, K, Li) crystallize in a monoclinic structure [6–8]. Materials for $n=3$ or 4 consist of $(Ti_3O_7)^{2-}$ layers held together by alkali-metal ions (Na^+, K^+). With a low alkali metal content ($n=6$–8), they show a tunnel structure and exhibit a good chemical stability [7]. The phase diagram of the system Na_2O–TiO_2 shows the presence of $Na_2Ti_3O_7$ and $Na_2Ti_6O_{13}$ as well as $Na_2Ti_6O_{13}/TiO_2$ [9–11]. The lattice parameters for $Na_2Ti_3O_7$ [12] and $Na_2Ti_6O_{13}$ [13] previously reported by Anderson et al. are given in the Table 1.

Previous studies were focussed on the compounds synthesized by solid state reactions from TiO_2 and Na_2CO_3 or Na_2O [2,3,6,9–11]. Sodium titanates can also be synthesized by hydrothermal reaction of TiO_2 with NaOH [14,15]. The sol–gel method using alkoxide precursors [16] was also applied to directly obtain $Na_2Ti_3O_7/Na_2Ti_6O_{13}$ and $Na_2Ti_6O_{13}/TiO_2$ mixtures for sensor devices. The mixing ratio of $Na_2Ti_3O_7/Na_2Ti_6O_{13}$ was 3:1 in mass ratio and a qualitative estimation on the mixture $Na_2Ti_6O_{13}/TiO_2$ gave a higher mixing ratio.

The aim of the present work is to improve the sol–gel route to synthesize pure phases of $Na_2Ti_3O_7$ and $Na_2Ti_6O_{13}$ and to characterize the structural and electrical properties of the samples as function of sintering parameters in order to better understand the behavior of sodium titanate mixtures. Dilatometry,

*Corresponding author. Laboratoire d'Electrochimie et de Physico-Chimie des Matériaux et des Interfaces, Ecole Nationale Superieure d' electrochimie et d' electrometalluregie de Grenoble, Institut National Polytechnique de Grenoble, Equipe Interfaces en Electrochime, des Solides, FR 38402, Saint Martin d'Hères Cedex, France. Fax: +33 4 76 82 66 70.
E-mail address: christian.lopez@lepmi.inpg.fr (C. Lopez).

0022-4596/$ - see front matter © 2004 Elsevier Inc. All rights reserved.
doi:10.1016/j.jssc.2004.09.008

Table 1
Lattice parameters

Compound	$Na_2Ti_3O_7$	$Na_2Ti_6O_{13}$	TiO_2
Crystalline structure	Monoclinic	Based-centered monoclinic	Tetragonal
JCPDS	31–1329	73–1398	78–1509
Cell parameters	$a=9.12790$ Å $b=3.80320$ Å $c=8.56210$ Å $\beta=101.6°$	$a=15.1310$ Å $b=3.7450$ Å $c=9.1590$ Å $\beta=99.30°$	$a=b=0.4594$ Å
Spatial group	$P21/m$	$C2/m$	$P4_1/mnm$

thermogravimetry analysis (TGA), differential thermal analysis (DTA), X-ray diffraction (XRD) and scanning electronic microscopy (SEM) were used. Electrical properties of the samples were investigated by Electrochemical Impedance Spectroscopy (EIS) in different atmospheres (air, argon and air–CO_2).

2. Experimental

2.1. Preparation of materials

$Na_2Ti_3O_7$ and $Na_2Ti_6O_{13}$ were separately prepared by a sol–gel method. The starting compounds were titanium (IV) *n*-butoxide (99%, Jansen Chimica), sodium hydroxide (99%, Strem Chemical Inc.), butanol-1 (Chimie plus lab.) and distilled water. The alkoxides were mixed in a butanol medium (1:1 volume ratio) and the sodium hydroxide was dissolved in distilled water (1:25 mass ratio). The aqueous NaOH solution was added simultaneously with an excess of distilled water to the alkoxide solution in order to obtain a fast hydrolysis-condensation reaction. All the reagents were initially heated between 55 and 60 °C, as described in [16]. In this previous work, the mixture was finally heated at 100 °C to evaporate water and residual alcohol. In the present work, the drying step was improved. This mixture was stirred under heating until a gelatinous solution was obtained, and then dried by lyophilization for 4 days. The sol is freezed at −40 °C under 0.12 mbar. In such conditions, the powder is slowly dried by a shift of the solid–gas water equilibrium. This method leads to a powder with a small amount of agglomerates.

The synthetic powders were directly heated in air at different temperatures in the range 773–1373 K for 4–16 h with a heating rate of 4 °C min^{-1}. If necessary (for dilatometry, SEM and electrical analyses), the powders, calcined or not calcined, were then uniaxially (100 MPa) and isostatically (250 MPa) pressed into pellets of different diameters. The pellets of $Na_2Ti_3O_7$ and $Na_2Ti_6O_{13}$ were sintered at 1323 K for different periods.

2.2. Characterizations

2.2.1. XRD analysis

X-ray powder diffraction patterns were obtained at room temperature using a Siemens D500 with Cu$K\alpha_1$ radiation ($\lambda=1.5405$ Å) and 2θ scanning rate of 0.4° min^{-1} from 10° to 80°.

2.2.2. SEM analysis

The particle morphologies of sodium titanates were observed with a scanning electron microscope (SEM) LEO 440 equipped with a tungsten filament.

2.2.3. Dilatometry analysis

These analyses were carried out in order to study the shrinkage of the pellets using an ADAMEL LHOMARGY® D.I.24 dilatometer. The different powders, calcined or not calcined at different temperatures under air, were pressed into cylinders of 8 mm diameter and a few millimeters in thickness.

2.2.4. Thermogravimetric and differential thermal analysis

TGA and DTA were carried out in dry air, using a Setaram TGA 24S16 instrument. The temperature range was 300–1373 K, with a heating and a cooling rate of 10 K min^{-1}.

2.2.5. Electrical characterization

Electrochemical impedance spectroscopy (EIS) measurements were carried out using an impedance analyzer HP 4192A in a two electrode cell (platinum electrodes) with an amplitude of 0.02 V in the frequency range 5–10^6 Hz. For these analyses, synthesized powders were first calcined at 1073 K for 4 h in air. These powders were then pressed and sintered at 1323 K for 1 h in the case of $Na_2Ti_3O_7$ and 2 h for $Na_2Ti_6O_{13}$ to finally obtain pellets of 12 mm diameter and a few millimeters in thickness. On each side of the pellets, Pt ink (Engelhard 6926) was painted and sintered at 1023 K for 2 h in air. The electrical conductivity of these compounds was determined as a function of the temperature and the gas atmosphere. An electrochemical pump-gauge device was used to adjust the oxygen partial pressure at different values between air and argon ($10^{-5}<P(O_2)<10^{-1}$atm).

3. Results and discussion

3.1. XRD patterns

Depending on the heat treatment, $Na_2Ti_3O_7$, $Na_2Ti_6O_{13}$ and TiO_2 phases were observed and identi-

fied using the JCPDS files (Table 1). The phases detected by XRD analyses are summarized in Tables 2 and 3.

With the synthesized powder $Na_2Ti_3O_7$, a single phase of $Na_2Ti_3O_7$ is observed after heating at temperatures lower than 1373 K. After calcinations at 1373 K, for 4 or 6 h, $Na_2Ti_3O_7$ is partially decomposed into $Na_2Ti_6O_{13}$. The proportion $Na_2Ti_3O_7$ wt%/$Na_2Ti_6O_{13}$ wt% decreases with the duration of the heat treatment: 80/20 for 4 h and 70/30 for 6 h. These proportions were determined by the ratio between the characteristic peaks of $Na_2Ti_3O_7$ (11° and 26°) and the $Na_2Ti_6O_{13}$ ones (12° and 25°). A calcination temperature of 1073 K for 4 h has been chosen because this temperature allows obtaining a well-defined $Na_2Ti_3O_7$ compound.

With the synthesized powder $Na_2Ti_6O_{13}$, XRD patterns show that a single phase of $Na_2Ti_6O_{13}$ can be observed for temperature below 973 K. Above 973 K, some characteristic peaks of TiO_2 (rutile) are detected. This TiO_2 phase is also observed in the literature in the case of solid-state synthesis [17]. However, only a qualitative analysis can be carried out from the XRD pattern, because the crystallographic structures of TiO_2 and $Na_2Ti_6O_{13}$ are different. In the following, a sintering temperature of 1073 K for 4 h was used for $Na_2Ti_6O_{13}$ as for $Na_2Ti_3O_7$. In such conditions, considering the simultaneous presence of $Na_2Ti_6O_{13}$ and TiO_2 phases, we will designate this material $Na_2Ti_6O_{13}/TiO_2$.

The present results slightly differ from the previous ones [16] probably due to the drying process of powders, which was now performed at lower temperatures.

3.2. Shrinkage studies

For the determination of the sintering parameters, pellets with 8 mm diameter were pressed and used to follow the shrinkage of the compounds. In many cases, the initial powders were initially heated at different temperatures (973/1073/1173 K) to study the influence of the calcination temperature.

The results obtained with $Na_2Ti_3O_7$ are summarised in Fig. 1. With the not calcined powder, two shrinkage processes are observed, the first one around 400 K and the second around 900 K. With the powder initially calcined at 773 K, only the second shrinkage process is observed. Indeed, the first one can correspond to the evaporation of water and the residual products of intermediate reactions, which were produced during the sol–gel synthesis. The nature of the phenomena

Table 3
Evolution of the $Na_2Ti_6O_{13}$ phase as a function of sintering conditions detected by XRD studies

Prescribed compound	Experimental conditions	Phase detected by XRD
$Na_2Ti_6O_{13}$	773 K/4 h	Not crystallized
	873–973 K/4 h	One phase $Na_2Ti_6O_{13}$
	1073 K/4 h	$Na_2Ti_6O_{13}$ + TiO_2 (rutile)
	1173–1273 K/4 h	
	1273 K/16 h	
	1323 K/10 h	
	1373 K/4 h	
	1373 K/6 h	

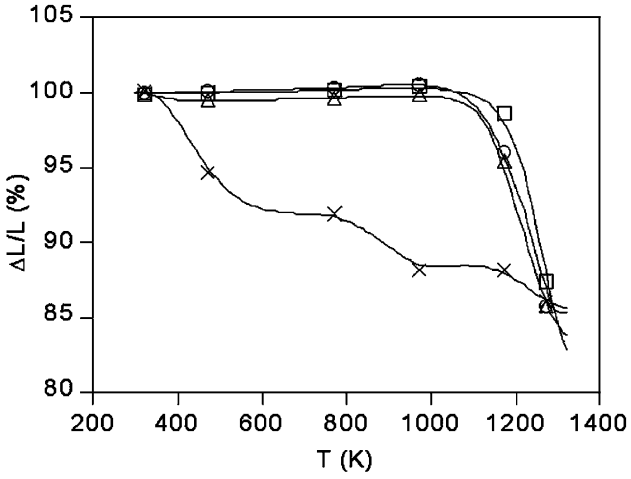

Fig. 1. Dilatometry curves obtained with $Na_2Ti_3O_7$: (×) not calcined (△) calcined 973 K/4 h, (○) calcined 1073 K/4 h, (□) calcined 1173 K/4 h.

Table 2
Evolution of the $Na_2Ti_3O_7$ phase as a function of sintering conditions detected by XRD studies

Prescribed compound	Experimental conditions	Phase detected by XRD	Proportion (%)
$Na_2Ti_3O_7$	773–873 K/4 h	Not crystallized	—
	973 K/4 h	$Na_2Ti_3O_7$ + Unknown phase	
	1073 K/4 h	One phase $Na_2Ti_3O_7$	
	1173–1273 K/4 h		
	1273 K/16 h		
	1323 K/10 h		
	1373 K/4 h	Two phases $Na_2Ti_3O_7$ + $Na_2Ti_6O_{13}$	80–20
	1373 K/6 h	Two phases $Na_2Ti_3O_7$ + $Na_2Ti_6O_{13}$	70–30

corresponding to the second shrinkage process was not precisely determined, however the XRD pattern of $Na_2Ti_3O_7$ showed that the crystallization of the phase occurs around 900 K. Otherwise, the thermogravimetric study presented in the following part underlines a weight loss at similar temperature. With samples calcined at 973 K and higher temperatures, only the shrinkage of the pellet is observed above 1100 K. In order to obtain dense pellets (around 85–90% of the theoretical density), a sintering temperature of 1323 K for 1 h was used for $Na_2Ti_3O_7$. We have verified that no secondary phase appeared during this thermal treatment.

With the $Na_2Ti_6O_{13}/TiO_2$ raw powder (not calcined), two shrinkage processes are also observed, but the first one is less marked than for $Na_2Ti_3O_7$, as shown in Fig. 2. These two shrinkage processes have the same signification than in the previous compound. With $Na_2Ti_6O_{13}/TiO_2$ powder initially calcined at 973 K and higher temperatures, similar results are obtained. The shrinkage of the pellet also started around 1100 K. A sintering temperature of 1323 K for 2 h was used to obtain dense pellets of $Na_2Ti_6O_{13}/TiO_2$.

This study shows that no dense pellet of pure $Na_2Ti_6O_{13}$ can be obtained for sintering temperature below 1073 K. Above 1073 K, TiO_2 additional phase occurred.

3.3. Thermogravimetric and differential thermal analyses

These analyses were performed in air on $Na_2Ti_3O_7$ and $Na_2Ti_6O_{13}/TiO_2$ mixtures, which were not initially calcined. Results are shown in Fig. 3(a) and (b).

With the $Na_2Ti_3O_7$ precursory powder, two weight losses are observed by TGA corresponding to two peaks on DTA (Fig. 3a). An important weight loss (about 15%) occurs with the first one (around 400 K) and an endothermic peak appears simultaneously on DTA. This was explained by the evaporation of water and organic reaction residues. For the second weight loss (about 5%), an exothermic peak around 950 K appears corresponding to the formation of the $Na_2Ti_3O_7$ phase previously observed by XRD analysis from 973 K (Table 2) and suggested by dilatometry experiment (Fig. 1).

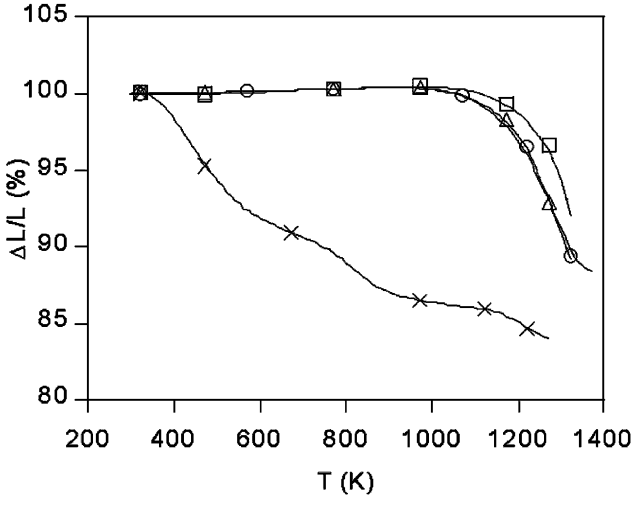

Fig. 2. Dilatometry curves obtained with $Na_2Ti_6O_{13}/TiO_2$: (×) not calcined, (△) calcined 973 K/4 h, (○) calcined 1073 K/4 h, (□) calcined 1173 K/4 h.

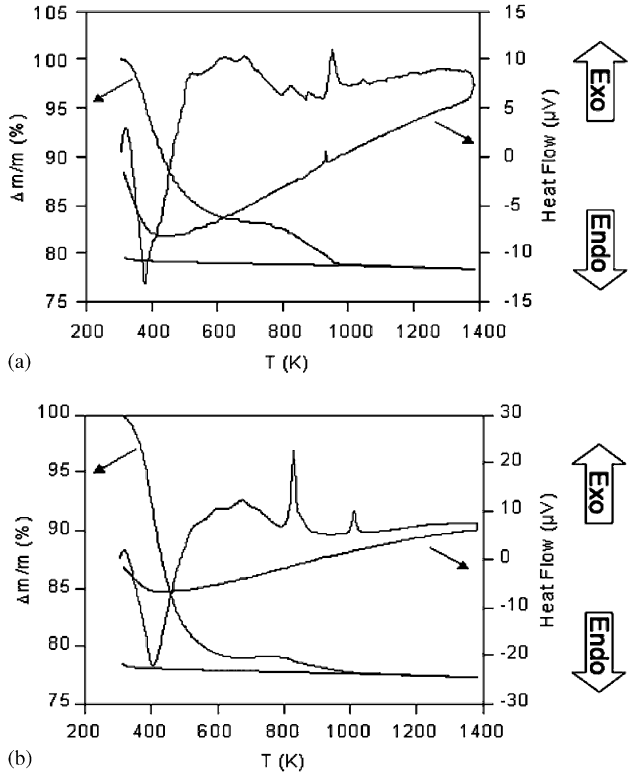

Fig. 3. Thermogravimetric and differential thermal analysis results obtained with: (a) $Na_2Ti_3O_7$, (b) $Na_2Ti_6O_{13}/TiO_2$.

With the $Na_2Ti_6O_{13}/TiO_2$ precursory powder, three steps are observed by TGA and three peaks on DTA (Fig. 3b). The first one around 400 K corresponding to a weight loss of 21% seems to be due to the evaporation phenomena as in the $Na_2Ti_3O_7$ case. As the same time, an endothermic peak is present on DTA. A second weight loss of 1.2% occurs around 830 K simultaneously to an exothermic peak, which was identified as the $Na_2Ti_6O_{13}$ phase crystallization previously located below 873 K by an XRD study (Table 3) and dilatometry analyses (Fig. 2). A third weight loss about 0.5% can be observed at 1000 K corresponding to another small exothermic peak. As mentioned previously, XRD study revealed the presence of TiO_2 phase (rutile) above 973 K (Table 3). This latter peak can be associated with the transformation of a small amount of $Na_2Ti_6O_{13}$ in TiO_2.

In these two cases, the second weight loss, around 850–900 K, occurring simultaneously with the phase

crystallization, could be explained by the hydroxyl groups elimination. These OH groups, located at the solid surface, need high temperature to be eliminated [19,20].

3.4. SEM analyses

The effect of the shrinkage process on the microstructure of $Na_2Ti_3O_7$ and $Na_2Ti_6O_{13}/TiO_2$ is illustrated by SEM.

The SEM micrographs of $Na_2Ti_3O_7$ powder heat-treated at 1073 (below shrinkage temperature) or 1273 K (above shrinkage temperature) for 4 h are shown in Fig. 4. The heat-treated powder (Fig. 4b) shows an interpenetrating aggregation of polygonal structures, being several micrometers in length and around 500 nm in thickness, after shrinkage according to the literature data [12,18]. A similar study was performed for $Na_2Ti_6O_{13}/TiO_2$ heat-treated at 1073 or 1273 K for 4 h and results are shown in Fig. 5. Above the shrinkage temperature (Fig. 5b), we have only observed the expected growth and agglomeration behavior of the microstructure. Comparing to the SEM micrographs of the Fig. 4, the polygonal structure observed in the case of $Na_2Ti_3O_7$ is not obtained here.

The scanning electron micrographs of $Na_2Ti_3O_7$ pellets are given in Fig. 6. The synthesised $Na_2Ti_3O_7$ powder was first sintered at 1073 K for 4 h, after that a pellet was prepared and sintered at 1323 K for 1 h (Fig. 6a) or for 10 h (Fig. 6b). Micrograph (a) shows a fusion like structure of $Na_2Ti_3O_7$ revealing a common sintering behavior whereas a non-homogeneous structure is observed on micrograph (b), with length and thickness superior to 15 μm, when the sintering time is longer. Sintering for 10 h at 1323 K seems to catalyze the coalescence of $Na_2Ti_3O_7$ polygons into very large structures.

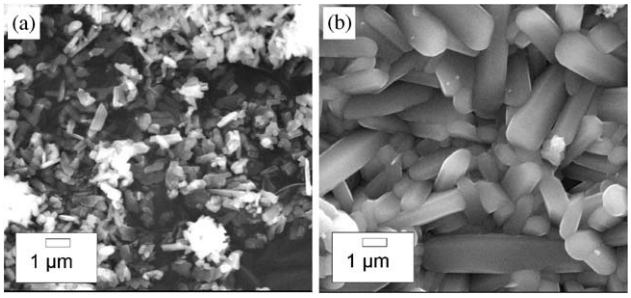

Fig. 4. SEM micrograph of heat-treated $Na_2Ti_3O_7$ powder: (a) sintered at 1073 K-4 h, (b) sintered at 1273 K-4 h.

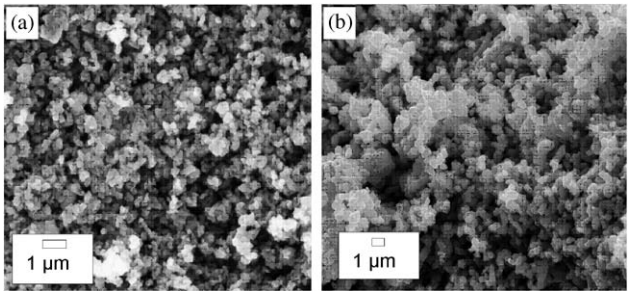

Fig. 5. SEM micrograph of $Na_2Ti_6O_{13}/TiO_2$ powder: (a) sintered at 1073 K-4 h, (b) sintered at 1273 K-4 h.

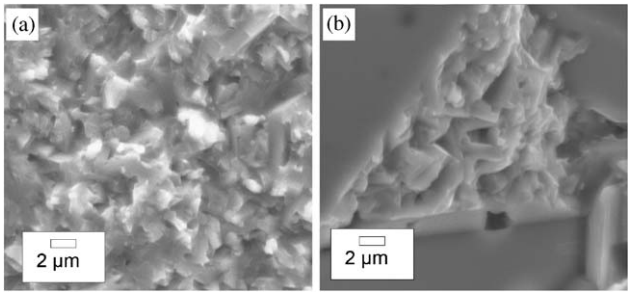

Fig. 6. SEM micrograph of $Na_2Ti_3O_7$ pellet: (a) pellet calcined at 1323 K/1 h, (b) pellet calcined at 1323 K/10 h.

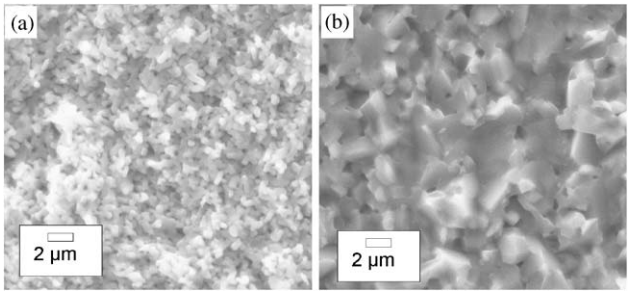

Fig. 7. SEM micrograph of $Na_2Ti_6O_{13}/TiO_2$ pellet: (a) pellet calcined at 1323 K/2 h, (b) pellet calcined at 1323 K/10 h.

Similar studies were carried out with $Na_2Ti_6O_{13}/TiO_2$. The scanning electron micrographs of $Na_2Ti_6O_{13}/TiO_2$ pellet are given in Fig. 7. The micrograph (a) shows spherical agglomerates of $Na_2Ti_6O_{13}/TiO_2$ around 0.5 μm in diameter. A heated time of 10 h at 1323 K (Fig. 7b) allows the growth and the coalescence of the spherical agglomerates leading to a fusion like structure. Contrary to $Na_2Ti_3O_7$, no important large structure is observed.

3.5. Electrical properties

These analyses were carried out by EIS on samples of $Na_2Ti_3O_7$ and $Na_2Ti_6O_{13}/TiO_2$. No measurements on pure $Na_2Ti_6O_{13}$ were possible because samples were not sufficiently dense. On the impedance diagrams, the grain and the grain boundary contributions were not sufficiently separated to determine the bulk conductivity of $Na_2Ti_3O_7$ and $Na_2Ti_6O_{13}/TiO_2$. So the total resistance, i.e., the intersection of the diagram with the real axis at

low frequencies, was used to calculate the total conductivity using two softwares packages (Zview© and Eqvcrt©). Fig. 8 shows typical impedance diagrams for $Na_2Ti_3O_7$.

Figs. 9 and 10 show the temperature dependence of the conductivity of $Na_2Ti_3O_7$ and $Na_2Ti_6O_{13}/TiO_2$ pellets, respectively, under pure oxygen, air and argon. The conductivity of $Na_2Ti_3O_7$ follows an Arrhenius behavior with an activation energy about 0.79 eV. No variation of the conductivity with the oxygen partial pressure was observed with this compound. The conductivity of $Na_2Ti_6O_{13}/TiO_2$ also follows an Arrhenius behavior under air and pure oxygen, with an activation energy around 0.9 eV. As shown in Fig. 10, two slopes are observed on $Na_2Ti_6O_{13}/TiO_2$ under argon. The modification of the slopes is probably due to the presence of TiO_2 whose electronic conductivity contributes at low oxygen pressures. Our results are in good agreement with the values obtained by Pasierb et al. [17] using EIS method. They strongly differ to the results obtained by dc-measuremens [4] for which chemical diffusion can be responsible. The activation energy values for all the samples are summarized in the Table 4.

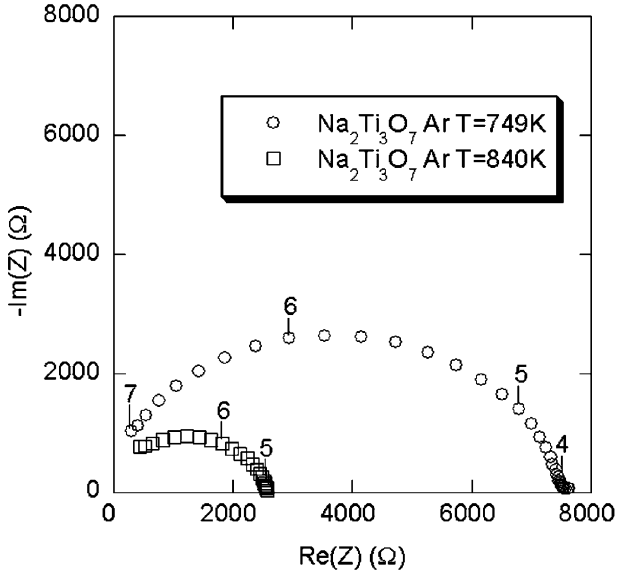

Fig. 8. Impedance diagrams measured with $Na_2Ti_3O_7$ under argon at 749 and 840 K.

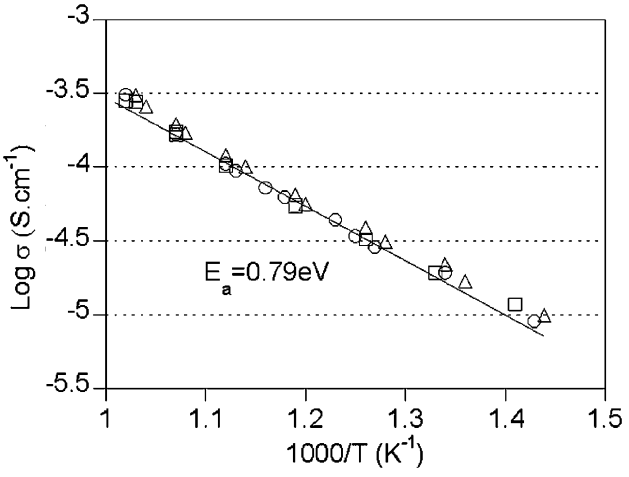

Fig. 9. Electrical conductivity of $Na_2Ti_3O_7$ as a function of temperature under (○) O_2, (□) air and (△) argon.

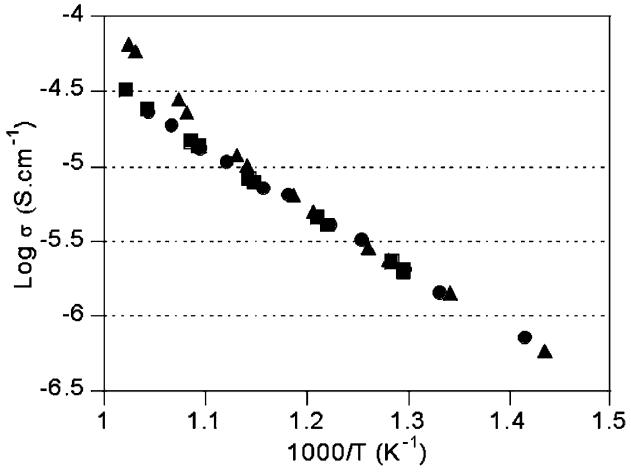

Fig. 10. Electrical conductivity of $Na_2Ti_6O_{13}/TiO_2$ as a function of temperature under (●) O_2, (■) air and (▲) argon.

Table 4
Activation energies

Component	Atmosphere	Ea (eV)
$Na_2Ti_3O_7$	O_2	0.79
	Air	0.79
	Ar	0.79
$Na_2Ti_3O_7$-10	Air	0.8
	Ar	0.8
$Na_2Ti_6O_{13}/TiO_2$	O_2	0.88
	Air	0.92
	Ar	0.97
$Na_2Ti_6O_{13}/TiO_2$-10	Air	0.68
	2.5%CO_2-air	0.69
	Ar	0.72

In all the studied experimental conditions, the conductivity of $Na_2Ti_3O_7$ is higher than the $Na_2Ti_6O_{13}/TiO_2$ one, with a factor of 10 (Figs. 9 and 10). This result is in agreement with some previous studies realized on $Na_2Ti_3O_7/Na_2Ti_6O_{13}$ and $Na_2Ti_6O_{13}/TiO_2$ mixtures [16], in which the conductivity was higher for larger $Na_2Ti_3O_7$ contents than with the $Na_2Ti_6O_{13}/TiO_2$ one.

In order to study the effect of sintering time, Fig. 11 shows the temperature dependence of the total conductivity of $Na_2Ti_3O_7$ in air sintered for 1 h, $Na_2Ti_3O_7$ sintered for 10 h ($Na_2Ti_3O_7$-10), $Na_2Ti_6O_{13}/TiO_2$

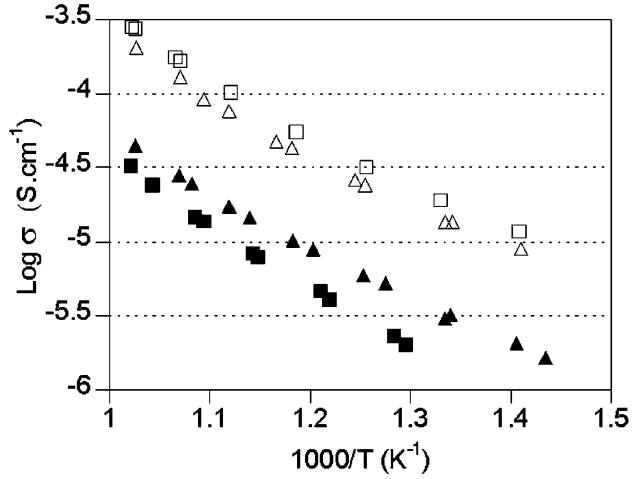

Fig. 11. Electrical conductivity of $Na_2Ti_3O_7$ (□), $Na_2Ti_3O_7$-10 (△), $Na_2Ti_6O_{13}/TiO_2$ (■) and $Na_2Ti_6O_{13}/TiO_2$-10 (▲) as a function of the temperature under air.

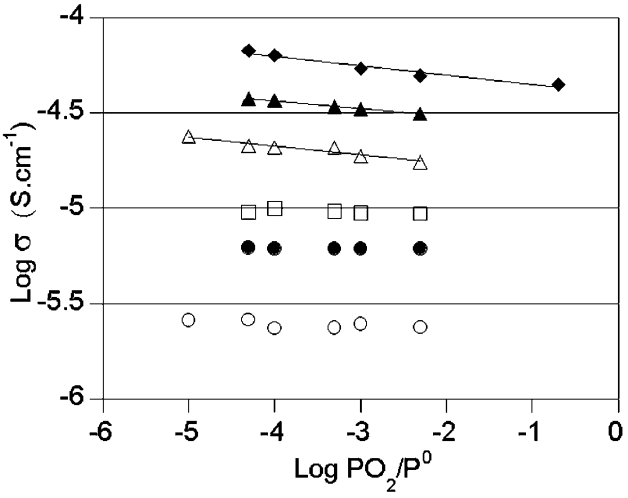

Fig. 12. Oxygen partial pressure dependence of the conductivity of $Na_2Ti_6O_{13}/TiO_2$: (○) $Na_2Ti_6O_{13}/TiO_2$ 799 K, (□) $Na_2Ti_6O_{13}/TiO_2$ 889 K, (△) $Na_2Ti_6O_{13}/TiO_2$ 934 K and of $Na_2Ti_6O_{13}/TiO_2$-10: (●) $Na_2Ti_6O_{13}/TiO_2$-10 795 K, (▲) $Na_2Ti_6O_{13}/TiO_2$-10 936 K, (♦) $Na_2Ti_6O_{13}/TiO_2$-10 973 K.

sintered for 2 h and $Na_2Ti_6O_{13}/TiO_2$ sintered for 10 h ($Na_2Ti_6O_{13}/TiO_2$-10) at 1323 K. We observe only linear dependencies when measurements were made under air but a similar discrepancy as in Fig. 10 occurred for measurements under argon at high temperatures. The sintering time at 1323 K has two different influences on the conductivity of the samples. For $Na_2Ti_3O_7$, the conductivity of $Na_2Ti_3O_7$-10 is slightly lower than the one obtained for short sintering duration. As previously shown on the micrograph (Fig. 6b), $Na_2Ti_3O_7$-10 is composed of large structures, which perhaps constrict the conductivity pathways or modify the conductivity mechanism, but with similar activation energy. On the contrary, the conductivity of $Na_2Ti_6O_{13}/TiO_2$-10 is higher than the $Na_2Ti_6O_{13}/TiO_2$ one. XRD pattern of these compounds showed approximately a constant ratio between $Na_2Ti_6O_{13}$ and TiO_2. On the micrograph of $Na_2Ti_6O_{13}/TiO_2$-10, we have also observed that the agglomerates are larger than in $Na_2Ti_6O_{13}/TiO_2$ (Fig. 7). This observation is characteristic of a sintering process. This phenomenon corresponds to a coalescence of the grains, which results in a packing, a reduction of porosity and, in our case, an increase of the total conductivity of this material. The variations of the conductivity of $Na_2Ti_6O_{13}/TiO_2$ and $Na_2Ti_6O_{13}/TiO_2$-10 as function of the oxygen partial pressure for temperatures above 900 K, as shown in Fig. 12, can also be explained by the presence of TiO_2. As it is well known, the conductivity of TiO_2 depends on oxygen pressure. This dependence is not observed in the $Na_2Ti_3O_7$ case. On the impedance diagrams of $Na_2Ti_6O_{13}/TiO_2$-10, whatever the atmosphere used (O_2, air or Ar), for a temperature higher than 773 K, an additional loop was observed at low frequencies, as shown in Fig. 13. This additional contribution is characterized by a capacity of

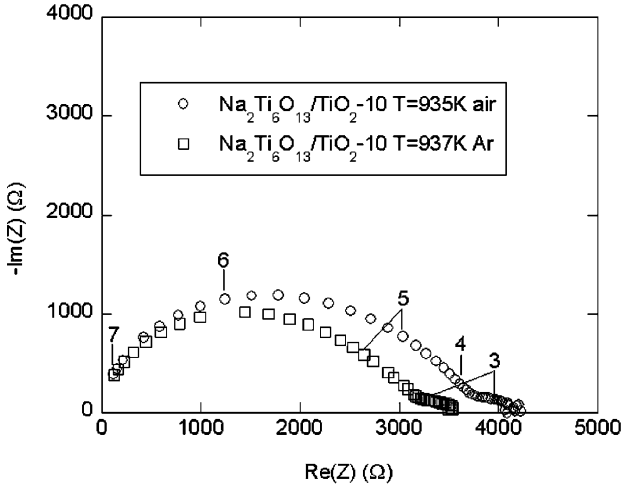

Fig. 13. Impedance diagrams measured with $Na_2Ti_6O_{13}/TiO_2$-10 under air and argon.

about 10^{-7} F cm^{-2} and a relaxation frequency around 10^3 Hz. Ramirez et al. [16] have also obtained similar results with a mixture of $Na_2Ti_6O_{13}$ and TiO_2. They also proposed that this contribution was due to the presence of TiO_2. Pasierb et al. [17] modeled their results with a homogeneous approach taking into consideration that both the bulk and grain boundaries have similar chemical composition. Even if the origin of the last contribution is not clearly defined, we could also suppose that this additional phenomenon results from the presence of TiO_2. In the present study, this additional loop is too small and cannot be clearly attributed. Nevertheless, it can be assumed that

$Na_2Ti_3O_7$ shows predominant ionic conductivity whereas $Na_2Ti_6O_{13}/TiO_2$ exhibits mixed conductivity especially at high temperatures whatever the sintering time is.

4. Conclusion

Pure $Na_2Ti_3O_7$ can be obtained by a sol–gel process up to a sintering temperature of 1373 K. For a higher temperature, it partially decomposed into $Na_2Ti_6O_{13}$, the proportion of these two phases depends on the sintering time. The morphology of samples shows some important large structures observed by SEM on pellets treated at high temperature for 10 h.

Pure phase $Na_2Ti_6O_{13}$ was obtained by the same sol–gel process only for temperatures around 973 K. After heat-treatment at 1073 K, some characteristic peaks of TiO_2 (rutile) were detected by XRD without formation of large structures.

In order to obtain dense pellets, the sintering temperature used for $Na_2Ti_3O_7$ and for $Na_2Ti_6O_{13}/TiO_2$ was 1323 K for 1 and 2 h, respectively. Whatever the temperature and the gas atmosphere were, the conductivity of $Na_2Ti_3O_7$ pure phase was higher than the $Na_2Ti_6O_{13}/TiO_2$ one. The total conductivity of $Na_2Ti_3O_7$-10 (sintered for 10 h) was lower than that of $Na_2Ti_3O_7$ whereas the conductivity of $Na_2Ti_6O_{13}/TiO_2$-10 was higher than the conductivity of $Na_2Ti_6O_{13}/TiO_2$. The decrease in conductivity of $Na_2Ti_3O_7$ with the sintering time could be a result of the formation of large structures. In the case of $Na_2Ti_6O_{13}/TiO_2$-10, a better densification seems to explain the increase of the conductivity, even if the content of TiO_2, which is a poor conductor, was constant. The dependence of the conductivity of $Na_2Ti_6O_{13}/TiO_2$-10 on the oxygen partial pressure at high temperatures seems to be due to the presence of TiO_2.

References

[1] R.D. Adams, R. Layland, M. Danot, C. Payen, Polyhedron 15 (1996) 2567–2571.
[2] J. Maier, M. Holzinger, W. Sitte, Solid State Ionics 74 (1994) 5–9.
[3] M. Holzinger, J. Maier, W. Sitte, Solid State Ionics 94 (1997) 217–225.
[4] M. Holzinger, J. Maier, W. Sitte, Solid State Ionics 86–88 (1996) 1055–1062.
[5] J. Ramirez-Salgado, P. Fabry, Sensors Actuators B 82 (2002) 34–39.
[6] T.P. Feist, S.J. Mocarski, P.K. Davies, A.J. Jacobson, J.T. Lewandowski, Solid State Ionics 28–30 (1998) 1338–1343.
[7] G.H. Li, J.M. Hong, Mat. Res. Bull. 34 (1999) 2341–2349.
[8] J.P. Shim, A.K. Lee, S.G. Park, J.S. Lee, Synthetic Metals 71 (1995) 2261–2262.
[9] R. Bouaziz, M. Mayer, C.R. Hebd, Seances Acad. Sci. Ser. C 272C (1971) 1874–1877.
[10] C. Gicquel, M. Mayer, R. Bouaziz, C.R. Hebd, Seances Acad. Sci. Ser. C 275C (1972) 1427–1430.
[11] C.E. Bamberger, G.M. Begun, J. Am. Ceram. Soc. 70 (1987) C-48–C-51.
[12] S. Anderson, A.D. Wadsley, Acta Crystallogr. 14 (1961) 1245–1249.
[13] S. Anderson, A.D. Wadsley, Acta. Crystallogr. 15 (1962) 194–201.
[14] K. Byrappa, B.S.R. Raj, V. Rajeev, A.B. Kulkarni, R.R. Clemente, S. Gali, Indian J. Phys. 71A2 (1997) 131–142.
[15] M. Watanabe, J. Solid State Chem. 36 (1981) 91–96.
[16] J. Ramirez, E. Djurado, P. Fabry, J. Eur. Ceram. Soc 24 (2004) 2477–2483.
[17] P. Pasierb, S. Komornicki, R. Gajerski, S. Kozinski, J. Electroceram. 8 (2002) 57–64.
[18] O.V. Yakubovich, V.V. Kireev, Crystallogr. Rep. 48 (2003) 24–28.
[19] H. Khireddine, P. Fabry, A. Caneiro, B. Bochu, Sensors Actuactors B 40 (1997) 223–230.
[20] J. Engell, S. Mortensen, L. Moller, Solid State Ionics 9/10 (1983) 877–884.